Magnetic phase diagram of $CeCu_2Ge_2$ up to 15 T: On the route to understand field-induced phase transitions

P. Geselbracht
Heinz-Maier-Leibnitz-Zentrum (MLZ), Technische Universität München, D-85748 Garching, Germany

A. Schneidewind
Jülich Centre for Neutron Science (JCNS) at Heinz-Maier-Leibnitz-Zentrum (MLZ), Forschungszentrum Jülich GmbH, Lichtenbergstrasse 1, D-85748 Garching, Germany

M. Doerr,[*] S. Granovsky,[†] M. Rotter,[‡] and M. Loewenhaupt
Institut für Festkörperphysik, Technische Universität Dresden, D-01062 Dresden, Germany

G. W. Scheerer and Z. Ren
University of Geneva, 24 Quai Ernest-Ansermet, CH-1211 Geneva 4, Switzerland

K. Prokeš
Helmholtz-Zentrum für Materialien und Energie (HZB), Hahn-Meitner-Platz 1, D-14109 Berlin, Germany
(Received 5 September 2016; revised manuscript received 25 April 2017; published 28 June 2017)

The features of the magnetic (H,T) phase diagram of $CeCu_2Ge_2$ are similar to those of superconducting $CeCu_2Si_2$, but the nature of these phases and transitions is still controversial. For $CeCu_2Ge_2$ we present results on electrical transport, thermodynamic measurements (magnetization, magnetostriction), and elastic neutron diffraction for fields up to 15 T parallel to the [110] direction. Two magnetic phases AF1, AF2 and a third, yet unidentified ferrimagnetic phase AF3 exist below $T_N = 4.2$ K and in fields up to approximately 26 T. At temperatures below 2.5 K a first-order transition from AF1 to AF2 at around 7.8 T was found experimentally, characterized by a shift of the observed propagation vector from $\mathbf{q_1} = (0.285\ -0.285\ 0.543)$ to $\mathbf{q_2} = (0.34\ -0.27\ 0.55)$. Above 12.5 T reflections belonging neither to the AF1 nor to the AF2 type were found. To interpret the macroscopic measurements and neutron data a mean-field simulation with the McPhase program was carried out, yielding a low-field double-$\mathbf{q}$ magnetic structure AF1 with $\mathbf{q_1}\pm = (0.278\ \pm 0.278\ 0.556)$ that jumps to AF2 with $\mathbf{q_2}\pm = (0.286\ \pm 0.286\ 0.545)$ at about 5 T (to be compared to the experimental value of 7.8 T). This transition is followed by a single-$\mathbf{q}$ structure AF3 with $\mathbf{q_3} = (0.28\ 0.28\ 0.56)$ at 10 T (as compared to 12.5 T from experiment) that is stable up to saturation at 26 T. These calculations also reveal the principal dependence of the experimental magnetization and susceptibility published earlier. The predicted single-$\mathbf{q}$ structure was not detectable by neutrons because of limitations in the employed scattering geometry.

DOI: 10.1103/PhysRevB.95.214425

I. INTRODUCTION

Many of the heavy-fermion compounds are characterized by the presence of long-range magnetic order and unconventional superconductivity [1]. Both effects can coexist or exclude each other which makes this class of compounds interesting to further investigations. A prominent example is the rare-earth-based heavy-fermion series $CeCu_2(Si,Ge)_2$. The properties of these isoelectric and isostructural tetragonal compounds have been extensively studied during the last decades. The parent compounds $CeCu_2Si_2$ and $CeCu_2Ge_2$ show an almost identical temperature-pressure phase diagram with the onset of superconductivity at ambient pressure and at ≈ 10 GPa, respectively [2]. Low-temperature and high-pressure properties are strongly related to quantum criticality, as discussed in [3,4].

$CeCu_2Ge_2$ orders antiferromagnetically below $T_N = 4.2$ K, a temperature that is slightly lower than the Kondo temperature $T_K = 6$ K [5]. This fact demonstrates the intermediate character between competing local Kondo behavior and long-range magnetic order. The zero-field magnetic structure below T_N is incommensurate with a propagation vector $\mathbf{q_1} = (0.28\ 0.28\ 0.54)$ and either described as a spiral [5] or as a sinusoidal spin-density wave [6]. The wave vector slightly shifts with decreasing temperature and locks-in at 1.5 K. The incommensurate zero-field magnetic structure was explained by the nesting properties of the calculated Fermi surface taking into account an itinerant component of the $4f$ moments of Ce^{3+} in addition to their local character [7]. Magnetic anomalies found by neutron scattering for single-crystalline $CeCu_2Ge_2$ at 0.2 K and about 8 T in the [110] direction are attributed to field-tuned quantum critical phenomena (QCP) [8]. New interpretations of neutron investigations, elastic as well as inelastic, are summarized in Refs. [9,10]. High-field magnetization measurements were carried out at 1.3 K for the crystallographic directions [100], [110], [001] and discussed

[*]doerr@physik.tu-dresden.de
[†]Also at Faculty of Physics, M. V. Lomonossov Moscow State University, 119991 Leninskie Gory, Moscow, Russia.
[‡]Also at Neutron Science Laboratory, Institute for Solid State Physics, University of Tokyo, Tokai 319-1106, Japan; McPhase Project, Dresden, Germany: http://www.mcphase.de

 ©2017 American Physical Society

in [11]. The saturation fields and the saturation moments were determined to be 15.5 T and 1.0 μ_B for the [001] direction and 27 T and (0.6 to 0.7) μ_B for the [110] and [100] directions, respectively. Metamagnetic transitions were observed at 7.8 T and 10.5 T for fields in the [110] and [100] directions, but none in the [001] direction. A modified phase diagram in the [100] direction containing two antiferromagnetic (AF1, AF2) phases and an intermediate phase up to saturation at about 27 T was reported in Ref. [12] based on magnetoelastic and magnetization measurements. Different values were obtained for the saturation fields along [100] of 35 T and of 31 T along [001] extrapolated from specific heat and resistivity measurements performed in moderate fields up to 14 T [13]. A more general magnetic (H,T) phase diagram was constructed in Ref. [14] using angle-dependent transport measurements covering the whole temperature and field region of the magnetically ordered phase of $CeCu_2Ge_2$. It shows a number of new phases, especially a modification of the antiferromagnetic ground state at about 10 T and subsequent phase transitions at 15 T and 23 T before saturation is reached at 30 T for fields in the [100] direction. Saturation for fields in the [001] direction is reached at 19 T. The reported suppression of thermal fluctuations at very low temperatures leads to interesting aspects of quantum criticality.

Despite many similarities in the published (H,T) phase diagrams, as for example the ordering temperature T_N or the clearly pronounced phase transition line between the phases AF1 and AF2 at about 8 T, blank areas and open questions still exist preventing a complete understanding of the heavy-fermion physics of $CeCu_2Ge_2$. More precisely, there is a lack of combining the experimental results with theoretical modeling or simulation. This would open a window to deeper insight into the interplay of the crystalline electric field (CEF), anisotropy of magnetic exchange, and Kondo physics in this class of 122 compounds. It is the aim of the present paper to use a complete set of existing and new data, thermodynamic (magnetostriction, magnetization), transport (resistivity), as well as elastic and polarized neutron investigations down to millikelvin temperatures and up to high pulsed fields, to construct and interpret microscopically the temperature and field areas of different magnetic phases in fields along the crystallographic [110] direction. The experimental work is accompanied theoretically; i.e., the features of the phase diagram are characterized with the help of a mean-field simulation by the McPhase program package. We demonstrate that in addition to the CEF anisotropy the main important prerequisite to reproduce the magnetic behavior in $CeCu_2Ge_2$ is the anisotropy in the magnetic two-ion coupling tensor.

II. SAMPLES AND METHODS

Experiments were performed on single-crystalline samples grown from Cu flux by a modified Bridgman technique [15]. For neutron scattering a large crystal of 3.5 g was available and had already been used in previous work [9,10,16]. Smaller samples for magnetization measurements were taken from a similar batch and cut into one cuboid with dimensions 3.0 × 3.0 × 2.5 mm^3 and a mass of 171 mg and a smaller one with 0.85 × 1.2 × 3.6 mm^3. Samples for resistivity measurements were grown independently and obtained by very slow cutting with a thin diamond saw to a thickness of 25 μm.

TABLE I. Applied current and magnetic field configuration of the three samples used for the resistivity experiment.

	Sample 1	Sample 2	Sample 3
$l \parallel I \parallel$	[110]	[110]	[100]
$H \parallel$	[110]	[001], [110]	[100]

A standard four-point technique was used to measure electrical resistivity as a function of temperature or field. The temperature control between 0.1 K and 6 K was carried out in a dilution fridge and in a ^{3}He fridge with superconducting magnets providing 8.5 T and 15 T, respectively (see Table I).

Magnetization experiments were performed in the temperature range 1.2 K to 300 K and in magnetic fields up to 14 T using an Oxford Instruments vibrating sample magnetometer. Additionally, the magnetic ac susceptibility was measured down to 0.4 K. These measurements were accompanied by magnetostrictive investigations to detect lattice effects due to magnetoelastic coupling. All striction experiments were performed in a high-resolution capacitive dilatometer [17] inserted into a variable temperature insert (VTI) of a cryomagnet for fields up to 15 T.

Neutron diffraction under field was performed at the E4 instrument at Helmholtz-Zentrum Berlin employing a 15 T vertical cryomagnet with a ^{3}He insert. The PG (002) monochromator provided a wavelength $\lambda = 2.4$ Å. Neutrons were collected by a 2D area detector. The sample was oriented in a scattering plane defined by $[1\bar{1}0]/[001]$. This allowed us to measure reflections of the type $(H\ -H\ L)$. The direction of the applied magnetic field is therefore [110], consistent with the definition of the field direction in our macroscopic measurements and our theoretical simulation. (Note the different definition of the field direction in our previous neutron experiments.) Scans were taken by in-plane sample rotation as a function of temperature at constant field or vice versa. The use of an area detector enabled us in contrast to our previous experiments to detect magnetic reflections that had a small component out of the scattering plane, i.e., with $(H\ -K\ L)$ and $|H| \neq |K|$. Characteristic data are 2D sets in $(2\Theta$-$\nu)$ space for each sample rotation. Peak positions are calculated by use of the UB matrix after integration over the rocking scan. $\nu = 0$ corresponds to the $(H\ -H\ L)$ scattering plane. In an additional experiment, the temperature dependence of the AF1 magnetic Bragg peak at zero field was studied on the time-of-flight spectrometer DNS (Heinz Maier-Leibnitz Zentrum, Garching). A PG (002) monochromator provided a wavelength of $\lambda = 4.2$ Å. The crystal was mounted in $[1\bar{1}0]/[001]$ orientation into a closed cycle cryostat with a ^{3}He insert. Intensity maps around the magnetic reflection were recorded at each fixed temperature, upon heating from base temperature to 10 K as well as upon cooling. The typical accuracies of the determined components of the propagation vectors are ±0.005.

III. EXPERIMENTAL RESULTS

For a first exploration of the (H,T) plane and of the existence of phase transitions we present measurements of

electric transport, magnetostriction, and thermal expansion together with the results of neutron diffraction. Transition temperatures were identified from anomalies such as kinks and bends in the above listed measurements or from their derivatives with respect to temperature or magnetic field.

A. Resistivity

Figures 1(a) and 1(b) present the temperature dependence of the resistivity ρ at different magnetic fields from 0 to 8.5 T for the field directions [110] and [001] and [100], respectively. At $T_N = 4.2$ K, the system becomes antiferromagnetic, shown by the characteristic resistivity anomaly. Fields of 8.5 T reduce T_N only by less than 0.2 K, more or less independently of the field direction. Above T_N a negative magnetoresistance is observed due to the field-induced suppression of the Kondo scattering. If the field is applied along the [001] axis one observes a 16% reduction at 8.5 T while for fields applied within the basal plane the reduction is only 5% at 8.5 T. In contrast, the system exhibits a strong positive magnetoresistance at low temperatures in the magnetically ordered regime. At 0.5 K, a field of 8.5 T increases the resistivity by roughly 50% of its zero-field value, more or less independently of the field direction. When the magnetic field is applied along [110], additional very weak S-like anomalies are observed in ρ-vs-T below T_N as indicated by the blue arrows labeled T_a in Fig. 1(a). They seem to emerge for low fields just below T_N and are shifted to lower temperatures with increasing field ($T_a = 2.8$ K at 8.5 T). At 8.5 T, a second S-like anomaly occurs at $T_b = 0.8$ K. None of these anomalies (T_a, T_b) are observed, when the field is applied along [100] or [001]. For fields up to 8.5 T the fitting parameter n for the temperature dependence of $\rho(T) = \rho_0 + A\,T^n$ shows no signatures of quantum criticality and no significant dependence on the field direction (the fitting parameter n is not shown here).

Figure 1(c) shows the field dependence of the resistance for the [110] direction for sample 2 in the field range 6 T $< H <$ 15 T. An S-shaped anomaly at $H_a = 9$ T and a steplike drop at $H_b \approx 8$ T correspond to the anomalies observed in the temperature dependence of the resistivity at T_a and T_b, respectively [Fig. 1(a)]. H_a is shifted to higher fields as the temperature decreases and we label this anomaly H_c for temperatures below 2 K. At the lowest temperature, $T = 260$ mK, two more steps in ρ are observed at $H_d = 8.7$ T and $H_e = 9.9$ T. The anomalies at H_a, H_b, H_c, H_d, and H_e are due to successive field-induced modifications of the magnetic order as partly observed by the neutron data discussed below. The narrow steps in the ρ-vs-H curve at H_b, H_c, H_d, and H_e at the lowest T indicate first-order transitions [10]. Similar anomalies in Figs. 1(a)–1(d) and Figs. 2 (top) and 2 (bottom) are characterized by the same index and color.

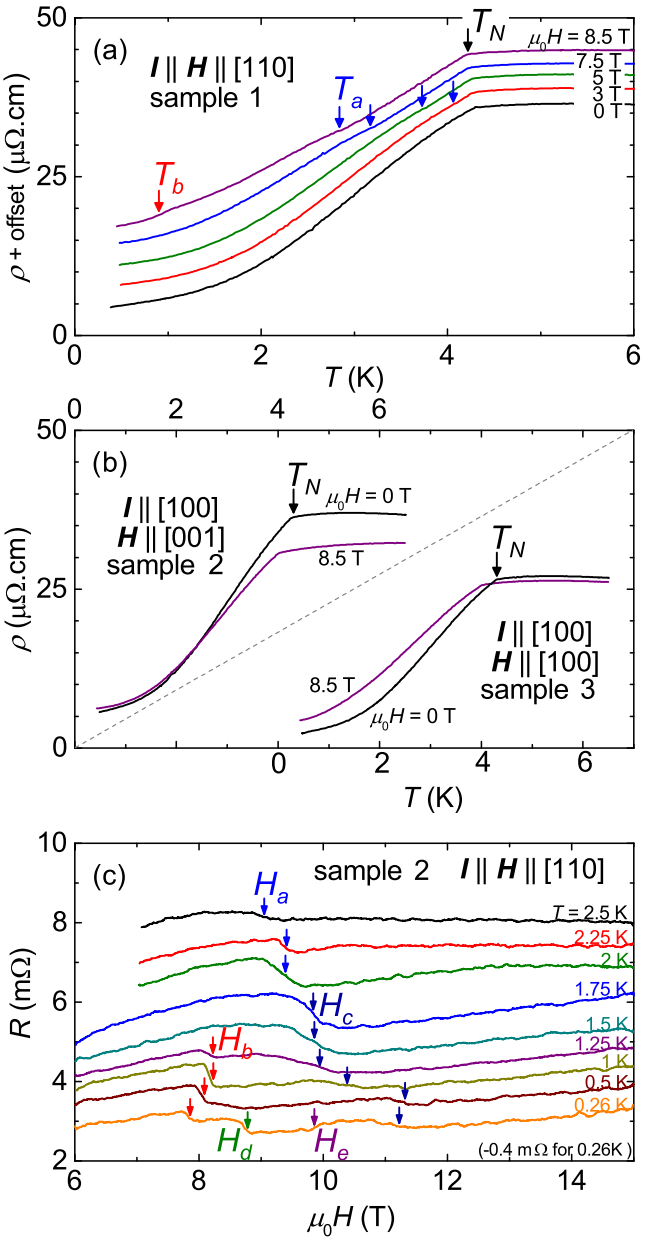

FIG. 1. Resistivity ρ of $CeCu_2Ge_2$ versus temperature T at different magnetic fields $\mu_0 H$ from 0 to 8.5 T, applied along (a) [110] and (b) [001] and [100]. For the sake of clarity, the curves for $\rho(T)$ in (a) are offset. There is no offset for $H = 0$. Arrows indicate anomalies corresponding to the Néel temperature T_N and to magnetic reconstructions inside the AF phase at T_a and T_b. (c) Resistance of sample 2 versus $\mu_0 H$ applied along [110] at temperatures from 0.26 to 2.5 K. Arrows indicate anomalies corresponding to field-induced transitions at H_a, H_b, H_c, H_d, and H_e; see text.

B. Magnetostriction

Figures 2 (top) and 2 (bottom) show for magnetic field in [110] direction the longitudinal (i.e., measurements parallel to the field direction) thermal expansion $dl/l(T)$ and longitudinal magnetostriction $dl/l(H)$, respectively. The graphs yield additional details about the phase transitions and the interplay of the magnetic and lattice subsystems. The results agree well with those of the magnetization (not shown here; compare with Ref. [12]). The thermal expansion curves for the temperature range from 2 K to 6 K and the field ranges from zero to 14 T exhibit two rather tiny changes in slope; the first one shifts from 2.7 K at 11 T to nearly T_N at low fields and is labeled T_a, and the second varies between 4.1 K and 4.4 K and is identified as the field dependence of T_N. Additional information about the phase diagram can be drawn from the

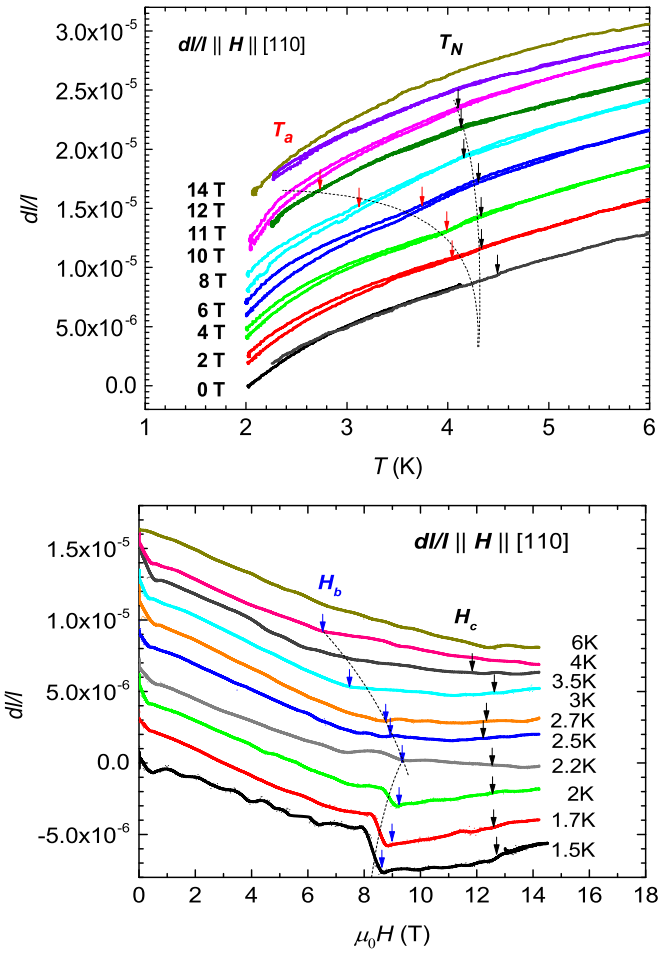

FIG. 2. Temperature dependence of the spontaneous longitudinal magnetostriction (top) and isothermal longitudinal forced magnetostriction (bottom) of single-crystalline $CeCu_2Ge_2$ for magnetic fields parallel to the crystallographic [110] axis.

field dependence of the forced magnetostriction measured for different fixed temperatures between 1.5 K and 6 K. Starting at the lowest temperature 1.5 K, two distinct transitions at about 7.8 T and 12.5 T can be observed, the first one characterized by a sharp drop of the sample length, the second one by a small increase in length. These two anomalies coincide quite well with the phase boundaries between AF1 to AF2 and AF2 to AF3. As the temperature is increased, the lower field anomaly weakens to a kink at continuously decreasing field values. The magnetostriction in the intermediate range is of hysteretic type in most of the curves pointing to an irreversible magnetic scenario within the AF2 phase. Combining all facts, it becomes also clear that the AF1 phase in nonzero magnetic field is not adjacent to the paramagnetic phase. All of the identified effects amount to less than 10^{-5} in relative changes of the sample length.

C. Neutron diffraction

In a previous paper [10] we already reported on the first-order phase transition from AF1 to AF2 at around 8 T at 30 mK. For clarity we again present here in Fig. 3 intensity maps around one magnetic Bragg peak. For fields lower than

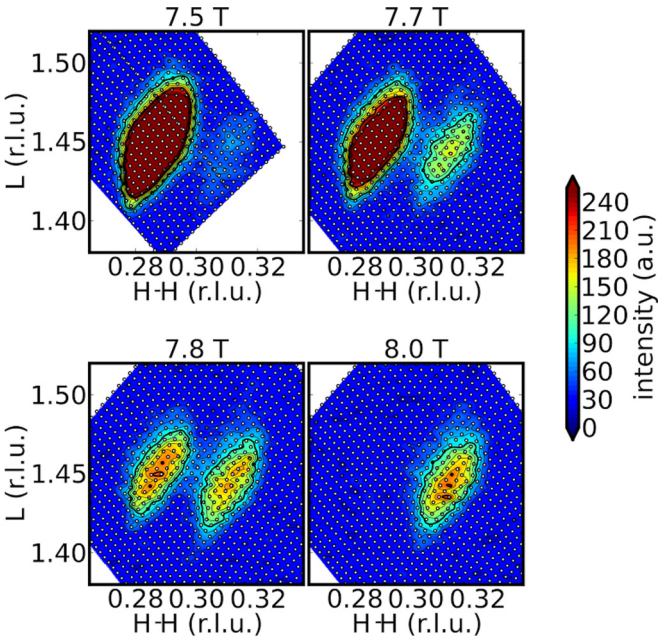

FIG. 3. Magnetic field dependence of the magnetic Bragg peak at $(H\ -H\ L)$ in a narrow field range around the phase transition from AF1 to AF2 at around 7.8 T. PANDA data from Ref. [10].

7.5 T the Bragg peak position corresponds to a propagation vector $\mathbf{q_1} = (0.285{-}0.285\ 0.543)$ that is still very close to its zero-field value at low temperatures. At 7.7 T, a second peak starts to rise and both peaks coexist at 7.8 T. Eventually at 8 T the peak corresponding to $\mathbf{q_1}$ has vanished. However, the new peak at 8 T could not correctly be characterized in this preliminary experiment. Employing an area detector in a subsequent experiment at E4 we found that the magnetic Bragg peak actually splits into two peaks, rotated by $\nu = \pm 1.5°$ out of the scattering plane as shown in Fig. 4. The two calculated peak positions (0.27 −0.34 1.45) (AF2 "upper") and (0.34 −0.27 1.45) (AF2 "lower") correspond to the new propagation vector $\mathbf{q_2}$ with (0.27 −0.34 0.55) and (0.34 −0.27 0.55) characterized by $|h| \neq |k|$. At 11.5 T only the "upper" peak, i.e., the peak with $\nu = +1.5°$, remains. The "lower" peak ($\nu = -1.5°$) has vanished. Figure 5 summarizes the field dependence of the intensity of the magnetic Bragg peak at $(H\ -K\ L)$ and of the three components ($h = H$, $-k = -K$, $l = L - 2$) of the corresponding propagation vector at low temperature (E4 data

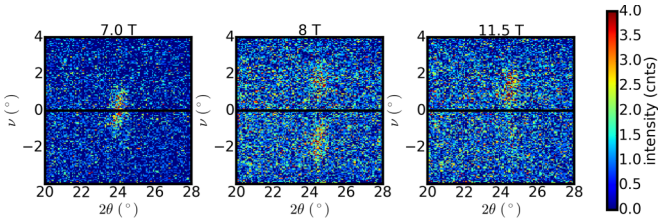

FIG. 4. Magnetic field dependence of the same magnetic Bragg peak as in Fig. 3 measured with an area detector at E4 at 0.3 K and for fields of 7, 8, and 11.5 T. Data are obtained as projection in 2 Θ-ν space. The horizontal line marks the scattering plane spanned by $[1\bar{1}0]/[001]$.

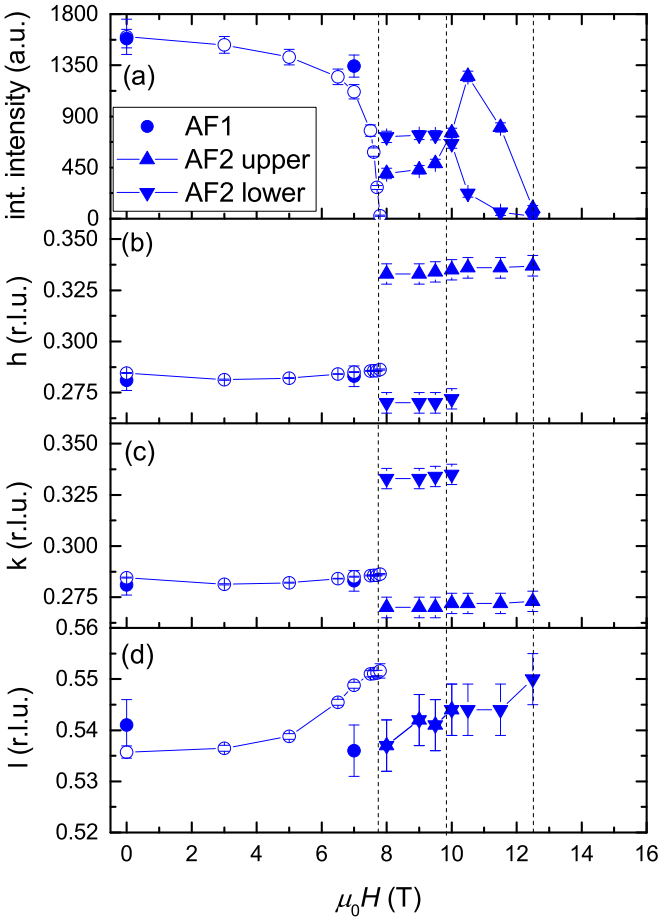

FIG. 5. Magnetic field dependence of the intensity of the magnetic Bragg peaks in AF1 and AF2 (a) and of the components h (b), $|k|$ (c), and l (d) of the corresponding propagation vector at 0.3 K obtained at E4 (filled symbols). Also shown are D23 data at 0.03 K for the AF1 phase (open symbols; taken from [10]).

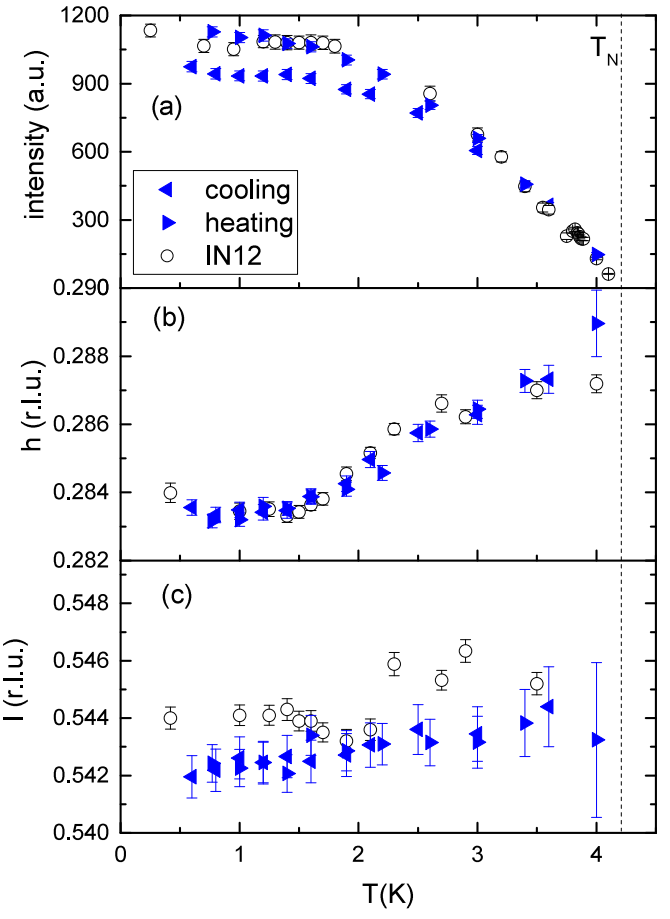

FIG. 6. Temperature dependence of the integrated intensity of the magnetic Bragg peak in AF1 for zero field (a), of $|h| = |k|$ (b) and l (c) components of the propagation vector measured at DNS (different filled symbols for heating and cooling) and IN12 (open symbols; data taken upon heating).

taken at 0.3 K: full symbols; D23 data taken at 0.03 K, only shown for AF1 phase: open symbols). The intensity as well as the propagation of the zero-field phase AF1 is stable up to 7 T. The AF1 peak is then replaced by the two peaks in AF2. The total intensity of the two AF2 peaks remains constant until 10 T. Here the "upper" peak gains in intensity, while the "lower" peak loses intensity. The components $|h| = |k|$ of the propagation vector remain nearly constant in AF1. The l component in the D23 experiment shows an upshift in AF1 that is not visible in the E4 data. The reason for this discrepancy is not clear. It could be due to either the lower temperature (0.03 K instead of 0.3 K) or an experimental artifact. At 12.5 T the AF2 peaks have vanished completely. Please note that the change of the two components h and k of the propagation vector from $|h| = |k|$ to $|h| \neq |k|$ when going from AF1 to AF2 cannot be caused by a lattice change. This can be inferred from the field dependence of selected nuclear Bragg peaks measured on D23 and reported in [10].

Figure 6 presents the temperature dependence of the intensity of the $(H - H\ L)$ Bragg peak (the same that is shown in Fig. 3 for 7.5 T) and of the corresponding propagation vector in zero magnetic field, i.e., in the AF1 phase. At $T_L \cong 1.5$ K the propagation vector locks-in to a constant value, as earlier reported [6]. In contrast to the behavior of the components of the propagation we observe a small hysteresis of the intensity: after heating to 10 K and cooling down again, approximately 10% of the intensity is not recovered. For the whole temperature range below T_N, a typical order parameter behavior is observed for the intensity without any anomaly. Fitting the empirical formula

$$I \propto [1 - (T/T_N)^{\alpha}]^{2\beta} \quad (1)$$

gives $\alpha = (2.6 \pm 0.3)$ and $\beta = (0.45 \pm 0.03)$. The values obtained here are close to those reported in [6] and β approaches the mean-field value $\beta = 0.5$. The empiric correction α is consistent with $\alpha = 2.7$ for $CePd_2Si_2$ [18].

IV. DISCUSSION

Figure 7 (left) presents the (H,T) phase diagram of $CeCu_2Ge_2$ for $H \parallel [110]$, established from resistivity (Fig. 1), magnetostriction (Fig. 2), and magnetization investigations together with information from our previous publication [12]. The observation or nonobservation of different types of magnetic Bragg peaks in neutron diffraction was used to distinguish between the phases AF1, AF2, and AF3 as

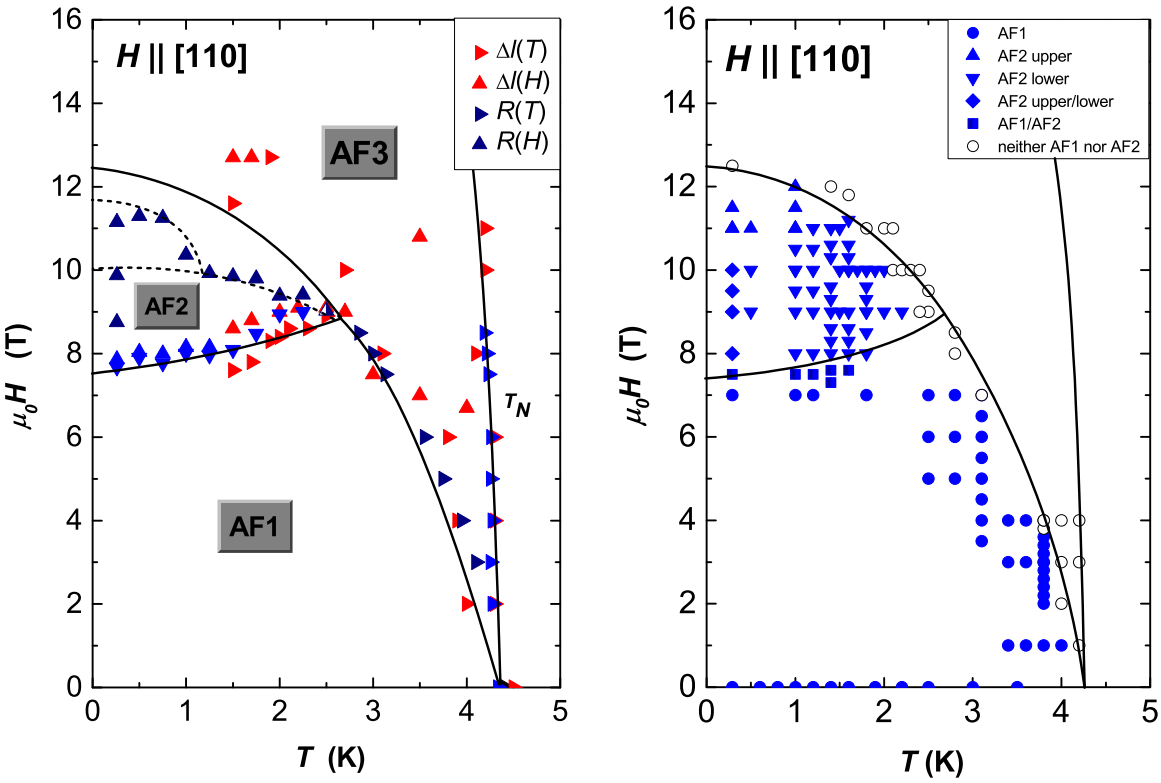

FIG. 7. Magnetic phase diagram of $CeCu_2Ge_2$ as a function of applied magnetic field along [110]. The data points in the left panel are taken from critical values of the resistivity, magnetization, and longitudinal magnetostriction indicating phase transition lines. The different symbols at different (H,T) values in the right panel indicate the positions of the neutron measurements and the observation or lack thereof of magnetic reflections related to the phases AF1 and AF2. The full lines are guides to the eyes separating the regions of the different phases AF1, AF2, and AF3 (compare [10]). The dashed lines indicate possible phase transitions within AF2.

presented in Fig. 7 (right). The magnetic ordering occurs at the Néel temperature $T_N = 4.2$ K and the transition is of second order. In the zero-field ordered state, the antiferromagnetic AF1 phase is characterized by an incommensurate magnetic propagation vector of the form $\mathbf{q_1} = (h\ -h\ l)$ with a moment direction perpendicular to this vector. The moment direction was determined by polarized neutron diffraction [19]. The temperature dependence of the $|h|$ and l components is given in Fig. 6. For example, a small shift of $|h|$ from 0.283 to 0.288 occurs between 0.5 K and the Néel temperature. The magnetic field dependence of the components at low temperature is shown in Fig. 5 for the phases AF1 and AF2. The zero-field phase, AF1, is stable up to 7.5 T. A first-order phase transition transforms it to another incommensurate phase, AF2, characterized by two magnetic Bragg peaks that lie out of the scattering plane (Fig. 4) and a propagation vector of the form $\mathbf{q_2} = (h\ -k\ l)$ with $|h| \neq |k|$. The observation of the two Bragg peaks related to two domains with $\mathbf{q_2}$ in AF2 is indicated in Fig. 5 and Fig. 7 (right) with different symbols: diamond for both AF2 "upper" and AF2 "lower", triangle-up for AF2 "upper", and triangle-down for AF2 "lower".

Our neutron diffraction experiments in the AF2 phase range indicate a change of domain population that results in a single-domain state at the upper limit of this range at about 12.5 T at which the magnetic satellites of the type $(h\ -k\ l)$ have vanished. This agrees with the hysteretic character of the magnetostriction in this range. It should be noted that the most important difference between a double-**q** structure and a single-**q** structure is the question of reversibility; i.e., whereas all effects are reversible in the first one, a field-induced single domain state should usually stay stable in the second one. Going up in field, the extended area of the AF3 phase above 12.5 T is reached where no magnetic satellites could be found by neutrons till now. From the following arguments we can assume that the yet unidentified phase AF3 is also of antiferromagnetic or, more precisely, of ferrimagnetic nature:

(i) The T_N line is continuous.

(ii) The anomaly in $\rho(T)$, typical for PM to AF transitions, does not change, even in the highest field.

(iii) At the transition fields $H_1 = 7.8$ T, $H_2 = 10$ T, and $H_3 = 12.5$ T, the resistivity shows only small steps and the field dependence of ρ almost does not change indicating similar carrier densities and mobilities for all three phases.

(iv) The magnetization increases linearly up to 26 T, with the exception of a small step at H_1 (see [11]).

Despite the uncertainty on the magnetic propagation vector of the AF3 phase the experimental data show the existence of a, possibly modified, AF3 phase down to zero field that occupies the space between the nonordered paramagnetic state above $T_N = 4.2$ K and the AF1 phase. This fact is also consistent with the behavior of the ac susceptibility published in [20]. There are clear similarities of the phase diagrams of $CeCu_2Ge_2$ for $H \parallel [100]$ [12,14] and for $H \parallel [110]$ (this paper). Thus by rotation of H around c one should observe continuity of the phase transition lines H_1, H_2, and H_3.

V. THEORY AND SIMULATION

In the absence of a complete theory of heavy-fermion antiferromagnets an analysis in the framework of a mean-field theory may provide useful information about the nature of the anisotropy and the magnetic interactions. Therefore, in order to interpret the experimental data we performed several model calculations using the McPhase 5.2 software suite [21]. Step by step the complexity of the model was increased in order to yield the observed magnetic properties, such as the magnetization and susceptibility, as well as the neutron scattering cross section.

First, a basic interaction which has to be considered is the crystal field. It tends to align the magnetic moments along [001] in $CeCu_2Ge_2$ [13,20] and $CeCu_2Si_2$ [22] as evidenced from susceptibility data. Therefore, a strong anisotropic magnetic exchange is necessary to force the moments into the basal plane. Moreover, from neutron spectroscopy it was found that the crystal field splitting is characterized by a doublet ground state and two excited doublets at 17 meV and 18 meV, respectively [16]. In our model for the low-temperature phase diagram we are concerned with temperatures below 5 K; therefore we may neglect the excited crystal field states and only consider the lowest Kramers doublet $|\pm\rangle$. Recently there have been vivid discussions about the orbital nature of this ground state and it has been demonstrated by NIXS measurements that in both $CeCu_2Si_2$ and $CeCu_2Ge_2$ the crystal-field ground-state doublet $|\pm\rangle$ is of the Σ type [23,24]. For our simulation we obtained the magnetic parameters of this doublet by extrapolating the experimental high-field magnetization [11] to zero, i.e., $M_c \sim 1.2 g_J\ \mu_B$ and $M_a = M_b \sim 0.6 g_J\ \mu_B$ (here $g_J = 6/7$ denotes the Landé factor of Ce^{3+}). In the frame of this crystal field approximation the Hamiltonian can be written as a sum of a general two-ion coupling and the Zeeman term

$$\mathcal{H} = -\frac{1}{2}\sum_{ij} J_i^{\alpha}\,\mathcal{J}_{\alpha\beta}(ij)J_j^{\beta} - \sum_i \mathbf{H}\cdot\mathbf{J}_i, \qquad (2)$$

where the $4f$ moment of the jth Ce^{3+} ion is represented by the three components of the angular momentum operator J_j^{α} ($\alpha = a,b,c$), which has only the following nonzero matrix elements: $\langle\pm|J_j^a|\mp\rangle = M_a/g_J$, $\langle\pm|J_j^b|\mp\rangle = \pm i M_b/g_J$, and $\langle\pm|J_j^c|\pm\rangle = \pm M_c/g_J$; compare with Ref. [25].

In the following steps the Hamiltonian (2) is treated by a mean-field theory as described in the review [21] and physical properties have been calculated with different parametrizations for the two-ion coupling tensor $\mathcal{J}_{\alpha\beta}(ij)$ with the aim to find the best representation of the observed magnetic properties. Thereby we arrived at some basic conclusions about the form and nature of the basic magnetic interactions in this system.

In order to obtain a magnetic structure with nonzero moments in the basal plane (as indicated by the peak in the experimental susceptibility along [100] at the Néel temperature), it is necessary to consider an anisotropy in the two-ion coupling: in our first attempt we set the component $\mathcal{J}_{cc}$ equal zero, $\mathcal{J}_{cc} = 0$, as well as the off-diagonal components of the interaction tensor and obtain the other components $\mathcal{J}_{aa} = \mathcal{J}_{bb}$ from a numerical variation with the aim to a maximize the Fourier transform $\mathcal{J}_{aa}(\mathbf{q}) = \mathcal{J}_{bb}(\mathbf{q})$ at the propagation vector $\mathbf{q_1} = (0.28\ 0.28\ 0.54)$:

$$\mathcal{J}_{\alpha\beta}(\mathbf{q}) = \sum_j \mathcal{J}_{\alpha\beta}(ij)e^{-i\mathbf{q}(\mathbf{R}_i-\mathbf{R}_j)}. \qquad (3)$$

Neighbors up to a distance of 10.652 Å were considered and restrictions given by space group symmetry were applied. In order to reproduce the measured low-temperature susceptibilities [13,20] we considered the screening of the $4f$ moment by the conduction electrons due to the Kondo effect. We did this by introducing an antiferromagnetic self-interaction

$$\mathcal{J}_{aa}(i=j) = \mathcal{J}_{bb}(i=j) = \mathcal{J}_{cc}(i=j) = -0.25\ \text{meV}.$$

From polarized neutron diffraction it has been concluded that the Fourier transform $\mathbf{m}(\mathbf{q})$ of the magnetic moments evaluated at the propagation vector $\mathbf{q} = (h\ h\ l)$ should point along $(1\ -1\ 0)$ [19]. This can be achieved by introducing a large enough in-plane anisotropy in the two-ion interaction, i.e., large off-diagonal components of the two-ion interaction $\mathcal{J}_{ab}$ and $\mathcal{J}_{aa} \neq \mathcal{J}_{bb}$. This will prevent a noncollinear (cycloidal) single-$\mathbf{q}$ magnetic structure with moments in the basal plane. Our simulations showed that for large enough in-plane anisotropy in the two-ion interaction the system chooses to minimize its free energy by forming a noncollinear double-$\mathbf{q}$ magnetic structure instead of a collinear magnetic structure. Though hitherto unknown in $CeCu_2Ge_2$ and similar systems, this finding is not completely new; in $GdNi_2B_2C$ it has already been shown that even the small anisotropy of the classical dipole interaction may trigger the formation of a double-$\mathbf{q}$ magnetic structure, if the ionic magnetic properties are isotropic [26]. In $CeCu_2Ge_2$ the crystal field anisotropy is large and such a noncollinear structure is unexpected. Because the doublet ground state is well separated from higher crystal field states (see above), the single-ion anisotropy within the ab plane, stemming from the crystal field, is quite small. Therefore the two-ion interactions will form noncollinear magnetic structures, if their (out of basal plane) anisotropy is strong enough to force the moments to be in the ab plane, which is not preferred by the crystal field in $CeCu_2Ge_2$. From experiment it is clear that the ordered moments are in the ab plane and therefore it is reasonable to expect that the two-ion interactions will exhibit significant anisotropy: $\mathcal{J}_{cc}$ has to be much smaller than the other components and it is therefore also likely that $\mathcal{J}_{ab}$ will be large and that $\mathcal{J}_{aa}$ and $\mathcal{J}_{bb}$ are quite different. Our simulations show that by increasing this two-ion in-plane anisotropy we get a transition from a cycloidal single-$\mathbf{q}$ to a double-$\mathbf{q}$ type of structure. Generally, such a behavior may be expected in any antiferromagnet for which the single-ion anisotropy does not force the moments into one particular direction. The observation of either a

(i) single-$\mathbf{q}$ cycloid or a
(ii) double-$\mathbf{q}$ structure

will depend on the magnitude of the anisotropy of the two ion interactions. In the double-$\mathbf{q}$ structure of $CeCu_2Ge_2$ the moments are in the basal plane and not collinear. However, for each propagation vector the magnetic structure factor components parallel to the projection of the propagation vector into the basal plane are very small in comparison to the components perpendicular to the propagation vector. This is in line with

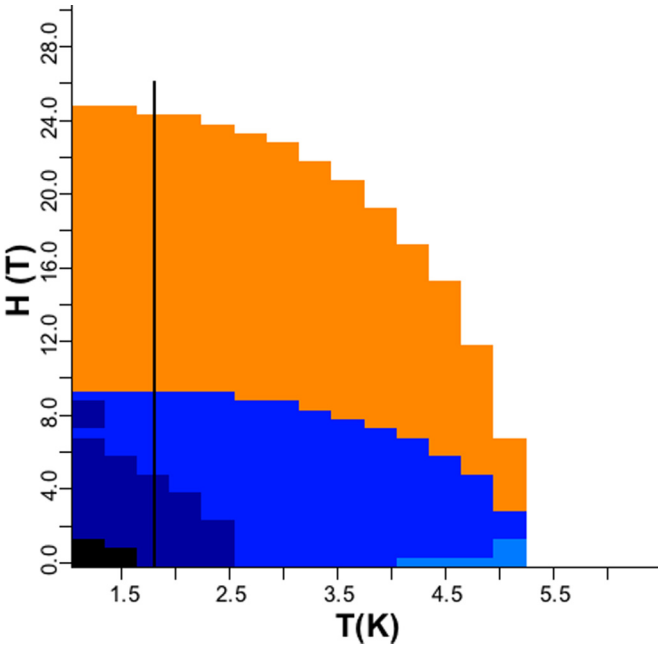

FIG. 8. Calculated magnetic phase diagram for applied field along the [110] direction. The double-**q** structures are shown in blue/black and the single-**q** structures in orange color. The black line at $T = 1.8$ K is a guide to the eye in connection with the following figures.

the observation from polarized neutron scattering that "the moments are perpendicular to the propagation vector". Thus we conclude that in the $CeCu_2Ge_2$ scenario (ii) is realized.

In order to obtain a good set of model parameters for $CeCu_2Ge_2$ about a dozen different two-ion interaction parameter sets were generated by variation of the nonzero components of the interaction tensor allowed by symmetry by keeping the in-plane anisotropy large enough to stabilize a double-**q** magnetic structure. Comparing now the calculated phase diagram, the propagation vector, the corresponding neutron intensities, and the bulk magnetization to the experimental data we chose the best parametrization. This model is presented here.

The model predicts double-**q** structures of the type (h $\pm h$ l) that exist in the blue-colored region of the magnetic phase diagram (Fig. 8), especially a propagation of $\mathbf{q_1}\pm = (0.278\ \pm 0.278\ 0.556)$ at 1.8 K and in zero field. Slight modifications of the h and l values as a function of temperature and magnetic field are indicated by lighter or darker blue coloring. The shift of h in AF1 (compare with Fig. 6) for its temperature dependence in zero field is well reproduced by the calculation yielding $h = 0.278$ for the low-temperature value (dark blue) and $h = 0.286$ for the higher temperature region (light blue). The double-**q** type of magnetic order is stable in a magnetic field up to 9 T. Above this field a single-**q** structure of type (h h l) is stabilized that exists in the orange-colored region of the phase diagram. The experimental findings in AF2 (h not equal k) cannot be reproduced by the present model. For a fixed temperature of 1.8 K the field dependence of the intensities of the corresponding magnetic reflections is presented in Fig. 9. The disappearance of the magnetic satellites in the experimental data at 12.5 T may

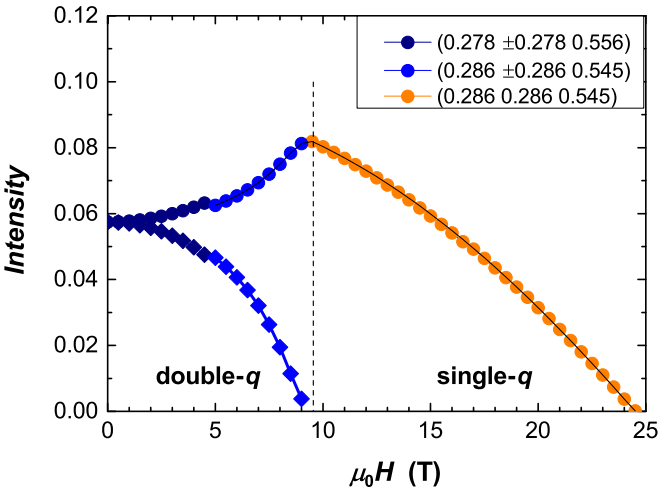

FIG. 9. Calculated field dependence of magnetic intensities for applied field along [110], $T = 1.8$ K. The larger intensities correspond to $\mathbf{q_{1+}}$ and cannot be observed in the (h $-h$ l) scattering plane; the smaller intensities correspond to $\mathbf{q_{1-}}$ and disappear at the double-**q** to single-**q** transition.

be interpreted in a natural way by the transition from the double-**q** to the single-**q** structure. This is the milestone of our model calculation in the understanding of the magnetic properties of $CeCu_2Ge_2$. Note that in the experiment in the [1 -1 0]/[001] scattering plane only the satellites of $\mathbf{q_{1-}} = (h\ -h$ $l)$ may be observed. Thus no peaks can be found in the single-**q** region. Though the general features of the magnetic properties of $CeCu_2Ge_2$ may be interpreted by the model calculation, there remain some quantitative discrepancies between the model calculation results and the experimental phase diagram such as a slightly different absolute value of the propagation vector and a smaller transition field to the single-**q** phase (9 T instead of 12.5 T in the experiment). Although currently hampered by computational possibilities it is likely that a further refinement of the interaction parameters may lead to an improved description of these features. Yet we note that the

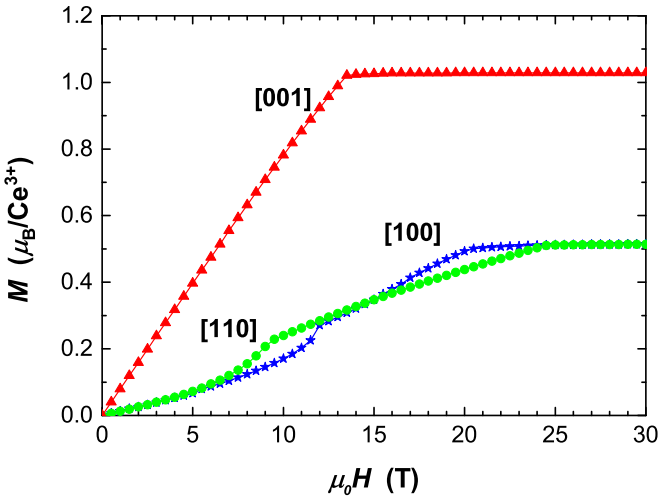

FIG. 10. Calculated magnetic moment for applied field along [100], [110], and [001] directions at $T = 1.8$ K.

absolute magnitude of these transition fields seems also to be sample dependent (compare [14]).

Finally, the temperature and field dependence of the magnetization has been calculated and is shown in Fig. 10. The transition from the double-**q** to the single-**q** phase for magnetic field in the basal plane is associated with a steplike increase in the magnetic moment at about 9 T along [110]. The calculation results are in good agreement with published magnetization data [11]. At high fields the moments saturate, because higher crystal field levels have been neglected in our model.

VI. CONCLUSIONS

In summary, we have mapped out the magnetic phase diagram of $CeCu_2Ge_2$ for a magnetic field direction along [110] by resistivity, magnetization, magnetostriction, and neutron diffraction experiments. Two magnetic phases, AF1 and AF2, were determined and analyzed by neutron scattering. In contrast, no magnetic reflections were found in the third phase, AF3. The behavior reveals the magnetic moments to be oriented in the basal plane consistent with all neutron scattering data. The [110] and [100] phase diagrams (see for example [12]) resemble each other indicating that the basal plane anisotropy is rather weak. A possible explanation of this finding comes out from a model calculation employing the McPhase program. Our numerical simulations show that large off-diagonal components of the two-ion coupling tensor may lead to a noncollinear double-**q** magnetic structure which is in accordance with the observation from our neutron diffraction experiments. The double-**q** structure becomes single **q** in a field along [110]. Due to the limitations of the used vertical high-field magnet to the $(h\ -h\ l)$ scattering plane only $\mathbf{q}_-$ reflections of the proposed double-**q** structures of AF1 and AF2 could be observed but no reflections of the proposed single-**q** structure of AF3. To test our suggestions one has to perform neutron diffraction employing a horizontal magnet:

(i) to check the behavior of the entangled **q** vectors of the double-**q** structure vs pure domain behavior of a single-**q** structure in AF1 and AF2;

(ii) to search for the single-**q** vector in AF3, unfortunately limited to the small region around 4 K and moderate fields up to 6 T.

The diverging slopes of the transition lines for $T \rightarrow 0$ and the fact that the transitions in the resistivity vs field curves at the lowest temperature are narrow steps are due to the first-order nature of the phase transitions as a function of field [10]. As usual, the ordering at T_N in zero field is of second-order character. Finally, the saturation along [110] was estimated to be achieved approximately between 25 T and 30 T.

The magnetic-field-induced change from a double-**q** to a single-**q** structure in $CeCu_2Ge_2$ also influences other physical properties. A model with modified exchange interactions should be useful for a comparison to $CeCu_2Si_2$.

ACKNOWLEDGMENTS

We wish to thank M. Deppe and C. Geibel (MPG CPfS Dresden) for providing us with the single-crystalline samples as well as HZB for the allocation of neutron radiation beamtime. P.G. thankfully acknowledges the financial support of HZB. Additionally, we gratefully acknowledge discussions with O. Stockert (MPG CPfS). The work was supported by HLD-HZDR, member of the European Magnetic Field Laboratory (EMFL). In this context, the activities of Z. S. Wang are especially acknowledged. The Geneva team acknowledges financial support from the Swiss National Foundation through Grant No. 200020-137519. Not least, we want to thank P. Schlottmann (FSU Tallahassee) for interesting discussions and a critical proofreading of the manuscript. The computation in this work has been done using the facilities of the Supercomputer Center, the Institute for Solid State Physics, the University of Tokyo.

[1] G. Knebel, D. Aoki, and J. Flouquet, C. R. Phys. **12**, 542 (2011).
[2] D. Jaccard and A. Holmes, Physica B **359-361**, 333 (2005).
[3] D. Jaccard, H. Wilhelm, K. Alami-Yadri, and E. Vargoz, Physica B **259-261**, 1 (1999).
[4] A. T. Holmes, D. Jaccard, and K. Miyake, Phys. Rev. B **69**, 024508 (2004).
[5] G. Knopp, A. Loidl, K. Knorr, L. Pawlak, M. Duczmal, R. Caspary, U. Gottwick, H. Spille, F. Steglich, and A. Murani, Z. Phys. B: Condens. Matter **77**, 95 (1989).
[6] A. Krimmel, A. Loidl, H. Schober, and P. C. Canfield, Phys. Rev. B **55**, 6416 (1997).
[7] G. Zwicknagl, J. Low Temp. Phys. **147**, 123 (2007).
[8] D. Singh, A. Thamizhavel, J. Lynn, S. Dhar, J. Rodriguez-Rivera, and T. Herman, Sci. Rep. **1**, 117 (2011).
[9] P. Geselbracht, E. Faulhaber, M. Rotter, K. Schmalzl, D. Quintero-Castro, O. Stockert, M. Loewenhaupt, and A. Schneidewind, Phys. Proc. **75**, 83 (2015).
[10] M. Loewenhaupt, P. Geselbracht, E. Faulhaber, M. Rotter, M. Doerr, K. Schmalzl, and A. Schneidewind, Phys. Proc. **75**, 230 (2015).
[11] K. Sugiyama, T. Miyauchi, Y. Ota, T. Yamada, Y. Oduchi, N. Dung, Y. Haga, T. Matsuda, M. Hagiwara, K. Kindo, T. Takeuchi, R. Settai, and Y. Onuki, Physica B **403**, 769 (2008).
[12] M. Doerr, S. Granovsky, M. Rotter, M. Loewenhaupt, A. Schneidewind, and Z. Wang, Phys. Proc. **75**, 572 (2015).
[13] T. Ebihara, Y. Sugiyama, Y. Narumi, Y. Sawai, K. Kindo, E. O'Farrell, M. Sutherland, and N. Harrison, J. Phys.: Conf. Ser. **391**, 012010 (2012).
[14] B. Zeng, Q. R. Zhang, D. Rhodes, Y. Shimura, D. Watanabe, R. E. Baumbach, P. Schlottmann, T. Ebihara, and L. Balicas, Phys. Rev. B **90**, 155101 (2014).
[15] M. Deppe, Ph.D. thesis, Technische Universität Dresden, 2004.
[16] M. Loewenhaupt, E. Faulhaber, A. Schneidewind, M. Deppe, and K. Hradil, J. Appl. Phys. **111**, 07E124 (2012).
[17] M. Rotter, H. Müller, E. Gratz, M. Doerr, and M. Loewenhaupt, Rev. Sci. Instrum. **69**, 2742 (1998).
[18] N. H. van Dijk, B. Fåk, T. Charvolin, P. Lejay, and J. M. Mignot, Phys. Rev. B **61**, 8922 (2000).

[19] P. Geselbracht, Ph.D. thesis, Technische Universität München, 2017.
[20] Y. Liu, D. Xie, X. Wang, K. Zhu, and R. Yang, Sci. Rep. **6**, 18699 (2016).
[21] M. Rotter, M. D. Le, A. T. Boothroyd, and J. A. Blanco, J. Phys.: Condens. Matter **24**, 213201 (2012); McPhase is available at http://www.mcphase.de.
[22] B. Batlogg, J. Remeika, A. Cooper, and Z. Fisk, J. Appl. Phys. **55**, 2001 (1984).
[23] J.-P. Rueff, J. M. Ablett, F. Strigari, M. Deppe, M. W. Haverkort, L. H. Tjeng, and A. Severing, Phys. Rev. B **91**, 201108(R) (2015).
[24] T. Willers, F. Strigari, N. Hiraoka, Y. Q. Cai, M. W. Haverkort, K.-D. Tsuei, Y. F. Liao, S. Seiro, C. Geibel, F. Steglich, L. H. Tjeng, and A. Severing, Phys. Rev. Lett. **109**, 046401 (2012).
[25] M. Rotter, M. Loewenhaupt, S. Kramp, T. Reif, N. M. Pyka, W. Schmidt, and R. v. d. Kamp, Europ. Phys. J. B **14**, 29 (2000).
[26] J. Jensen and M. Rotter, Phys. Rev. B **77**, 134408 (2008).